THESIS

DEVELOPING AN OPEN-SOURCE REMOTE SENSING FRAMEWORK FOR LONG-TERM WETLAND RESTORATION MONITORING

Submitted by

Jackson Akin

Graduate Degree Program in Ecology

In partial fulfillment of the requirements

For the Degree of Master of Science

Colorado State University

Fort Collins, Colorado,

Summer 2025

Master's Committee:

Advisor: Jessica O'Connell

Anna Armitage
Dave Koons

ABSTRACT

DEVELOPING AN OPEN-SOURCE REMOTE SENSING FRAMEWORK FOR LONG-TERM WETLAND RESTORATION MONITORING

Wetland restorations can take decades to show measurable success, yet long-term monitoring remains uncommon. Field-based monitoring is often costly and labor-intensive, making remote sensing an appealing alternative. In this project, we developed an open-source, reproducible remote sensing workflow calibrated with field data from a wetland restoration site in Galveston, Texas. The restoration was initiated in 2004, with additional efforts in 2011, with goals to increase wetland habitat, buffer wave energy, and slow the erosion of remaining natural marsh. Our objective was to build an automated monitoring framework to assess restoration trajectory over time using biophysical metrics, including elevation, land cover, and aboveground biomass. We trained models using Sentinel-2 satellite imagery and digital elevation model (DEM) data to estimate these metrics. To enhance elevation estimates, we developed a correction model that reduced root mean squared error (RMSE) from 0.29-m to 0.12-m. Our land cover model achieved an overall testing accuracy of 90% for classifying water, vegetation, and bare soil, while the aboveground biomass model performed with an RMSE of 82.4 g m^{-2} (normalized RMSE of 14%). These models were applied in time series analyses to evaluate site-wide landscape-level restoration progress. We found that restoration mounds of 20+ years old had lower elevations than reference sites, but were similar to mid-aged sites, suggesting they are relatively stable. Mounds also appeared to be buffering remaining natural areas from lateral marsh erosion. However, mounds created in 2004 showed increased rates of vegetation transitioning to water and should be monitored closely. By applying this scalable and cost-effective framework, managers can more readily detect emerging restoration challenges and make timely, data-driven decisions, such as planting more vegetation, implementing more erosion control structures, or increasing mound elevation through thin-layer soil placement. Through leveraging

high-resolution and freely available Sentinel-2 imagery and elevation data, the models achieved high classification accuracy and effectively captured key trends in biophysical parameters such as elevation, land cover and AGB, offering insight into restoration trajectories over time. While expert interpretation is still necessary for management decisions, this framework offers a powerful tool for improving long-term restoration monitoring and adaptive management.

ACKNOWLEDGMENTS

I would like to thank my advisor, Jessica O'Connell, for being a great guide and mentor through this process, and I am extremely grateful. I would also like to thank my lab at Colorado State as well as my committee members for being a great support group. Finally, I would like to thank my friends and family who always gave me confidence and belief throughout this research.

TABLE OF CONTENTS

1. INTRODUCTION

Wetland restoration helps to counteract degradation and habitat loss caused by human disturbance and climate change (Meli et al., 2014), but long-term monitoring is rare. This is important because wetlands provide ecosystem services such as carbon sequestration, wildlife habitat for migratory birds, and can serve as a flood buffer for the nearby urban areas (De Groot et al., 2018). Wetland restoration can restore ecosystem functionality and associated services (Tomscha et al., 2021), but requires long-term monitoring to guide effective decision-making. Monitoring differences in wetland area and elevation, through lateral or vertical expansion or erosion, as well as changes in vegetation productivity, allows managers to gauge wetland resiliency (Zhao et al., 2016). However, field work monitoring, while accurate, is expensive, time-consuming, and is rarely budgeted for long periods of time, and rarely covers broad landscapes evenly. To address this limitation, we have developed open-source remote sensing models and time series that offer a coastal marsh restoration monitoring approach that is both reproducible and efficient for spatiotemporal characterization.

Effective monitoring is essential for evaluating restoration outcomes, yet challenges remain in implementing large-scale assessments. National databases such as the National Wetland Condition Assessment and the National Wetland Inventory provide useful baseline data, but they often lack the detail needed for ongoing, localized management decisions (McCauley et al., 2019). Large-scale field work efforts can be resource and labor-intensive while also being limited spatially and temporally. However, small-scale field work efforts are still valuable in providing validation data for remote sensing modeling. Many restoration efforts focus on short-term success, with monitoring ceasing once positive results are observed due to funding and logistical constraints. This leaves long-term ecosystem function uncertain, a gap that remote sensing models can help fill (Shuman & Ambrose, 2003). This study aims to build remote sensing modeling tools that can be used to assess restoration success by linking field-based biophysical metrics to satellite-derived data. Freely available imagery and data from Sentinel-2 (S2)

satellites and light detection and ranging (LiDAR) missions can be utilized to create higher accuracy, custom monitoring tools. By integrating remote sensing with field measurements, we can track vertical and lateral marsh expansion or erosion through biophysical metrics, such as elevation, land cover, and aboveground biomass (AGB) over time and at a landscape level.

Restoration monitoring efforts must account for key biophysical indicators of vertical and lateral marsh changes. One such important indicator is wetland surface elevation. Elevation greatly impacts inundation frequency, and in turn, soil salinity and oxygen levels (Adam, 1993; Mendelssohn & Morris, 2000). Due to plants' different physiological tolerances to salinity and oxygen levels, plant communities change along elevation gradients from marsh interior to marsh edge (Bockelmann et al., 2002). This creates characteristic low and high marsh zones with distinct plant communities (Burger et al., 1997; Rasser et al., 2013). Many coastal wetlands have been impacted by land subsidence through groundwater withdrawal, increasing vulnerability to sea-level rise (White & Tremblay, 1995). Loss of elevation from land subsidence can alter many key functions that contribute to stability within wetland systems (DeLaune & Pezeshki, 1994). Wetland restoration often acts to counter land subsidence and maintain plant communities and elevation gradients, which are vital for stability and resilience in these ecosystems (Brasher & Blvd, 2015). Thus, cm-accurate estimation of elevation is important for tracking restoration success (Hladik et al., 2013). Paired with estimates of plant responses, such as plant cover and aboveground biomass, a more complete picture of wetland condition can be generated. Wetland plants themselves contribute to maintaining elevation because aboveground stems slow tidal waters and encourage sediment deposition, while root growth causes vertical soil accretion and reinforces soil structure (Krauss et al., 2014; Morris et al., 2002). Further, tracking land cover over time can reveal lateral shifts in key cover types such as vegetation, bare soil, and water, providing additional insight into marsh resilience, edge erosion, and habitat transitions (Giri et al., 2011; Guo et al., 2017; Schmidt & Skidmore, 2003).

We will test these techniques in Jumbile Cove in Galveston, TX, which is home to a long-term wetland restoration project that requires an efficient, large-scale monitoring solution. Galveston, TX is located on a barrier island along the Texas coast, and the Galveston Bay system is the seventh largest estuary in the United States. Wetlands in Jumbile Cove suffered degradation through land subsidence and have lost over 50% of their intertidal wetlands from 1930 to 1995 (Davis et al. 2024). Marsh restoration at Jumbile Cove began in 2004 and employed a mounded terracing technique designed to increase wetland acreage, buffer wave energy, slow erosion of remaining natural marsh, and provide habitat for a variety of organisms (Davis et al. 2024). These efforts aimed to restore critical ecosystem functions and services to both the wetland system and the surrounding community (Rozas & Minello, 2001). An additional restoration effort in 2011 expanded the project with new mounds constructed in a different part of Jumbile Cove. These restored areas, together with unmanaged natural marsh, offer a gradient of restoration ages that can serve as baselines for assessing restoration progress. These areas are hereafter referred to as Restoration Age Classes (RACs) and are categorized as reference (ref), mid-aged (mid), and old (old) RACs, respectively. This variation provides a unique opportunity to develop and apply remote sensing tools that assess wetland biophysical condition and track ecological trajectories over time.

Ecological monitoring through remote sensing requires careful selection of ground-truth and relevant remote sensing data for model building. Ground-truth field measurements are used to both validate and train open-source remote sensing models for dissemination to managers to track biophysical metrics. For remote sensing modeling, we relied on S2 satellites, LiDAR-derived digital elevation models (DEMs), and extreme gradient boosted machine learning algorithms. We created models in an open-source framework for relevant ecosystem characteristics, including land cover, elevation, and AGB. These models were used to generate time series and can be used to identify trends at a site-wide scale to view emergent patterns and generate well-informed management decisions. Managers can use these models and this monitoring framework to assess restorations on a larger scale that could have been previously limited by accessibility, time or funding restraints.

In this paper, our overall goal was to create an effective remote sensing monitoring method that can be used to track wetland restoration. To achieve this, our goals were first to assemble the datasets needed to begin model building. Next, we built open-source models for monitoring restoration progress. Finally, in order to test our model's ability to detect ecological trends for effective monitoring, we built remote sensing-derived time series to evaluate spatiotemporal differences between RACs of mounds in Jumbile Cove, Galveston, TX, as an example. This framework can help identify the spatiotemporal patterns and trajectories of RACs. We predict that wetland resilience will be indicated by similar mound elevations, an absence of decline in vegetation cover, and comparable AGB among RACs. Indicators of decline would start with the old RAC having significantly lower elevation than other RACs, which can increase flooding stress, and in extreme cases, include a consistent increase in bare soil or water cover, suggesting a conversion of vegetated marsh to mud flat or open water. This effort will assist with informing management on ecosystem function, reducing costs, improving restoration monitoring techniques, and increasing the likelihood of successful restorations.

2. METHODS

All pre-processing, modeling, and visualization steps were performed in R (R version 4.4.1, 2024-06-14).

2.1 Regional description and study site selection

Our study was conducted at wetland restoration sites and nearby unrestored areas within Jumbile Cove, Galveston Bay, TX, USA, (29.3013, -94.7950) (Figure 1). Tidal wetland restoration was established initially in 2004 (Figure 1). The restored areas were constructed using terrace and mound formations, created by piling dredged material in shallow bay areas and planting with native marsh vegetation. Initial plantings consisted solely of *Spartina alterniflora*, while *Batis maritima* and *Salicornia virginica* later colonized the marshes naturally. Our experimental design compared measurements at sites stratified by time since restoration (RACs), including reference marsh (natural, unrestored wetland), middle-aged

restoration mounds (10+ years since restoration), and old restoration mounds (20+ years since restoration). The ref RAC provided a baseline for characterizing healthy wetland functions. The mid and old RACs provided a space for time substitution that allowed us to determine if restoration results in functional improvements or declines through time. However, this approach may be confounded by spatial differences, such as variation in wind exposure across sites, that could independently affect ecological trajectories. By selecting all sites within the same cove, we aimed to reduce large-scale spatial variability, but some fine-scale spatial effects may still influence results. Specific study sites for inclusion within restoration age classes were randomly selected among the available sites within our main target study area, the Jumbile Cove.

This project also leveraged existing additional site data gathered in natural marsh in a similar coastal environment near Port Aransas, TX, as an effort to increase sample size for some types of models. Although these sites are hydrologically and geographically independent, they share similar tidal regimes, climate conditions, and dominant vegetation communities, making them ecologically comparable. The Port Aransas sites are natural marshes that were not restored or planted, in contrast to the constructed and planted marshes at Jumbile Cove. However, due to the nature of remote sensing models, which are sensitive to current surface conditions rather than a site's restoration status or management history, S2 data from these sites can be combined with data from restored sites for modeling purposes. When Port Aransas data were utilized, they were used exclusively to train the model, and Galveston data provided spatially independent data to validate model success (Section 2.3 below). Field data collected in Port Aransas, TX, included land cover estimates and elevation measurements, which were paired with coinciding Sentinel-2 reflectance and DEM elevation data. Biomass data were not collected at Port Aransas, and therefore, Port Aransas data were only used for training land cover and elevation models. By training in Port Aransas and testing in Galveston, we demonstrate that the model can be applied to similar geographies that it has not seen, showcasing the generality and robustness of the geospatial models. Model validation is described in Section 2.3.

Figure 1. Jumbile Cove wetland restoration sites. The old RAC (orange) was created in 2004, while the mid RAC (blue) began in 2011. The red polygon highlights the ref RAC, which is natural intact wetlands that serve as a baseline for wetland conditions.

2.2 Assemble the datasets needed for model building, including ground-truth and remote sensing data

We used field measures as ground truth data to inform remote sensing models that can evaluate restoration trajectory (Figure 2.1). Field visits took place once annually in early fall, which corresponds with peak biomass at the end of the growing season, and revisits occurred annually for three years in 2022, 2023, and 2024. Study sites were sampled during moderate tides, as boats are unable to access sites during the lowest tides, and high tides cover vegetation, increasing the difficulty of sample collection. To determine restoration site condition, we collected key biophysical metrics at each RAC for comparison. In fall 2022 and 2023, sampling focused intensively on one representative mound or reference marsh per RAC, whereas in 2024, data collection was less intensive but expanded spatially to include two to three mounds or reference marshes per RAC. Within each site, we established field plots stratified by elevation zones

that span a gradient from low (marsh edge) to high (marsh interior). These zones, from low to high elevation, encompassed mudflat, low marsh, and high marsh with 4-5 field plots per zone. At each field plot, we collected measurements of emergent plant cover, bare soil, and water cover, AGB, elevation, and water depth. Cover data was measured at each plot in 0.25-m^2 quadrats, and measured vegetation cover as a total and by individual plant species. AGB was collected at low and high marsh elevation zones in a 0.125 m^2 subplot within each vegetated field plot. Plant biomass was processed in the lab into live and dead vegetation and oven-dried at 80° C to a constant weight. We also measured elevation at each plot via a real-time kinematic (RTK) Trimble R12 Global Navigation Satellite System (GNSS) receiver (Trimble 2019), in the vertical datum NAVD88. These RTK orthometric heights (in meters) had a vertical accuracy of 15 mm and horizontal accuracy of 8 mm. Each plot was surveyed for three minutes, and 1 datapoint was collected per second, generating 180 elevation measurements total for each survey point.

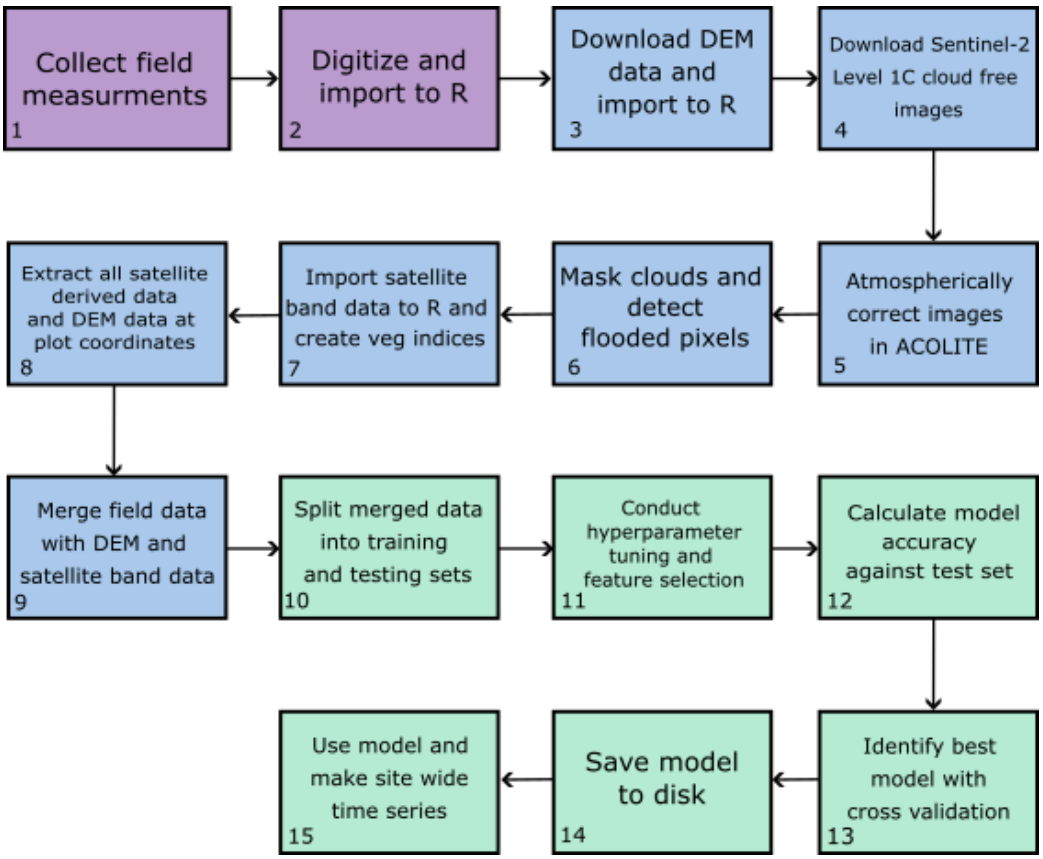

Figure 2. An outline of our general remote sensing model-building workflow. Colors represent field measurement steps (purple), data pre-processing steps (blue), and model-building steps (green). Steps are further detailed in the text.

To create remote sensing models, S2 imagery and LiDAR-derived DEMs were downloaded and used as predictors for the collected ground truth data (Figure 2.3). S2 satellites used the MultiSpectral Imager to collect reflectance in 13 spectral bands, ranging from 10-60 m spatial resolutions (Table 1), with a temporal resolution of 5 days. Low tide S2 imagery was downloaded from the European Space Agency's (ESA) Copernicus Dataspace Ecosystem (Figure 2.4) that was taken within 20 days of field measure collection dates. S2 Level 1C top of atmosphere reflectance images with less than 20% cloud cover were selected through a custom R script that requested batch images from the ESA OData API. After downloading images corresponding to the study area, the ACOLITE algorithm was used for atmospheric correction and cloud masking, as it was designed for processing images in water-dominant environments (Vanhellemont & Ruddick, 2016) (Figure 2.5). For Level 1C imagery, ACOLITE applied a threshold of 2.15% in the 1.6 μm SWIR band for non-water masking (Figure 2.6) and resampled all bands to 10-m spatial resolution. After importing images into R, vegetation indices (VIs) were created based on band formulas from previous literature (Figure 2.7) (Table 2). Additionally, simple ratios (SRs) were created based on the individual performance of bands in later models (Table 2). These indices were evaluated for importance through extreme gradient boosting-generated importance plots, derived from training data (detailed further in Section 2.3 below) (Figure 2.11). Reflectance and calculated indices were then extracted at each sample plot coordinate (Figure 2.8) and merged with field data from the same sample locations and sample dates within 15 days to create a dataframe for model building (Figure 2.9). DEMs were downloaded from the Texas Geographic Information Office (https://tnris.org/). DEM data collection took place from January 13th to March 22nd, 2018, as part of a project managed by Texas Strategic Mapping (Texas Geographic Information Office, n.d.). LiDAR data were collected using Riegl R680i and R780i sensors flown over 24,605 km², with a 1-m spatial resolution and a mean collection altitude of 732 m. DEM images were downloaded, imported into R, rasterized, then extracted and merged

with the model dataframe based on sample plot coordinates. Downstream modeling relied on this dataframe, which consisted of field measurements, satellite imagery, and DEM data.

Table 1. S2 bands, band names, wavelength midpoints, and spatial resolutions. S2 return frequency is 5 days over our study area.

S2 Bands	Band Names	Band Midpoint Wavelength (nm)	Resolution (m)
Band 1	Aerosol	443	60
Band 2	Blue	490	10
Band 3	Green	560	10
Band 4	Red	665	10
Band 5	Red Edge	705	20
Band 6	Red Edge	740	20
Band 7	Red Edge	783	20
Band 8	Near-Infrared	842	10
Band 8A	Red Edge	865	20
Band 9	Water Vapor	945	60
Band 10	SWIR-Cirrus	1375	60
Band 11	SWIR	1610	20
Band 12	SWIR	2190	20

2.3 Build remote sensing-derived models for monitoring restoration trajectory

We developed separate models to predict important biophysical metrics, including a digital elevation correction model (DECM), a land cover model (LCM), and an aboveground biomass model (AGBM). We created models for each attribute of interest through an extreme gradient boosting framework. S2-derived variables (reflectance, VIs, and SRs) were used as model predictors, with field-measured data serving as the response variable in model training and evaluation. Data was split into training and testing sets that comply with a spatiotemporal nested cross-validation (Schratz et al., 2019) (Figure 2.10). Data collected in the Port Aransas study was used as the training set for the LCM and DECMs, while Galveston data was utilized for the testing set. Splits within the training data were then used to conduct hyperparameter tuning to optimize model fitting (Figure 2.11). As part of the spatiotemporal nested cross-validation, hyperparameter tuning was informed only by the training subset and validated against withheld testing data (Figure 2.11). These training set splits were also used for model feature selection (i.e., selection of predictors), based on feature importance plots (Figure 2.11). Final model validation and accuracy assessment utilized only the testing subset, which was otherwise completely withheld from the

model-building process (Figure 2.12). Model accuracy calculated against the testing data for regression models was assessed through root mean squared error (RMSE) (1) as:

$$RMSE = \sqrt{\frac{\Sigma_{i=1}^{N}(y_i - \widehat{y}_i)}{N}} \quad (1)$$

Where *N* is the testing set sample size, y_i represents observed observations, and $\widehat{y}_i$ represents predicted observations. Error in regression models was also assessed using mean absolute error (MAE), shown as:

$$MAE = \frac{\sum_{i=1}^{n}\left|y_i - \widehat{y}_i\right|}{n} \quad (2)$$

Confusion matrices were used to evaluate classification models, like the LCM (Figure 2.12). From these, sensitivity, specificity, and overall accuracy were calculated to assess classification performance. Regression models were assessed post-hoc using the coefficient of determination shown below:

$$R^2 = 1 - \frac{\sum_i (y_i - \widehat{y}_i)^2}{\sum_i (y_i - \bar{y})^2} \quad (3)$$

Where y_i represents observed observations, $\widehat{y}_i$ represents predicted observations (Piñeiro et al., 2008), and $\bar{y}$ represents the mean of the observed data. Finally, we saved the model to disk as an object for use in future site-wide prediction (Figure 2.14).

Our modeling framework followed a consistent approach, but each model required specific methodological considerations based on the predicted variables. The LCM used the Port Aransas and Galveston dataset split, classifying S2 pixels as water, vegetation, or bare soil. This design resulted in using 65% of the data for training and 35% for testing. The DECM followed the same split but was applied only to elevations above 0 m NAVD88. The terrestrial (rather than bathymetric) LiDAR used in

the source data is rapidly attenuated by surface water and cannot be used in flooded areas. The elevation corrections are expected to be most useful in vegetated areas to reduce upward bias typical of short-statured vegetation in marshes (Hladik & Alber, 2012; Schmid et al., 2011). In contrast, the AGBM required a different data split, as biomass data was unavailable for Port Aransas. Instead, Galveston biomass data was split spatially, with mid and ref RACs used for training (65%) and old sites reserved for testing (35%).

Table 2. Remote sensing VIs and SR used in model building. Formulas are provided with the wavelength midpoint (ρ) instead of band names for easier translation between satellite platforms. Citations are provided for existing literature indices.

Index	Name	Formula	Citation
NDVI	Normalized Difference Vegetation Index[1]	$(\rho_{842}-\rho_{665})/(\rho_{842}+\rho_{665})$	Pettorelli et al. (2005)
NDWI	Normalized Difference Water Index	$(\rho_{560}-\rho_{842})/(\rho_{560}+\rho_{842})$	McFeeters (1996)
GARI	Green Atmospherically Resistant Index	$(\rho_{842}-(\rho_{560}-1.7*(\rho_{490}-\rho_{665})))/(\rho_{842}+(\rho_{560}-1.7*(\rho_{490}-\rho_{665})))$	Gitelson et al. (1996)
VARI	Visible Atmospherically Resistant Index	$(\rho_{560}-\rho_{665})/(\rho_{560}+\rho_{665}-\rho_{490})$	Gitelson et al. (2002)
BSI	Bare Soil Index	$(\rho_{1610}+\rho_{665})-(\rho_{842}+\rho_{490})/(\rho_{1610}+\rho_{665})+(\rho_{842}+\rho_{490})$	Chen et al. (2004)
NDRE	Normalized Difference Red Edge	$(\rho_{842}-\rho_{665})/(\rho_{842}+\rho_{665})$	Barnes et al. (2000)
AWEI	Automated Water Extraction Index	$4*(\rho_{560}-\rho_{842})-(0.25*\rho_{665}+2.75)$	Feyisa et al. (2014)
AWEISH	Automated Water Extraction Index Shadow	$\rho_{490+}2.5*\rho_{560}-1.5*(\rho_{842}+\rho_{1610})-0.25*\rho_{2190}$	Feyisa et al. (2014)
SR1	Simple Ratio 1	ρ_{842}/ρ_{490}	
SR2	Simple Ratio 2	ρ_{740}/ρ_{705}	
SR3	Simple Ratio 3	ρ_{842}/ρ_{443}	
SR4	Simple Ratio 4	ρ_{842}/ρ_{1610}	
PI	Phenological Index	$(\rho_{842}-\rho_{1610})/(\rho_{842}+\rho_{1610})$	O'Connell et al. (2017)
EVI	Enhanced Vegetation Index	$2.5*(\rho_{842}-\rho_{665})/(\rho_{842}+6*\rho_{665}+7.5*\rho_{490}+1)$	Jiang et al. (2008)

Index	Name	Formula	Citation
MTVI2	Modified Triangular Vegetation Index 2	$(1.5*(1.2*(\rho_{842}-\rho_{560})-2.5*(\rho_{665}-\rho_{560})))/sqrt((2*\rho_{842}+1)^2-(6*\rho_{842}-5*sqrt(\rho_{665}))-0.5)$	Haboudane et al (2004)
TCG	Tasseled Cap Greenness	$-0.3599*(\rho_{490})-0.3533(\rho_{560})-0.4734(\rho_{665})-0.6633(\rho_{842})+0.0087(\rho_{1610})-0.2856(\rho_{2190})$	(Shi & Xu, 2019)
gNDVI	Green Normalized Difference Vegetation Index	$(\rho_{842}-\rho_{560})/(\rho_{842}+\rho_{560})$	Pettorelli et al. (2005)

2.4 Generate remote sensing-derived time series to confirm observed spatial differences between restoration age classes.

Our third objective was to make annual site-wide predictions to observe spatiotemporal differences of biophysical metrics across mound age groups (Figure 2.15). Only one LiDAR collection was available during our study window, which did not provide the higher frequency time steps necessary to create a time series. Therefore, the DECM was left out of these steps, and we relied on RAC differences alone to understand elevation trajectories. For the LCM and AGBM, the batch download API script was used to acquire S2 Level 1C images of Jumbile Cove from 2016 to 2023 (the years of available S2 data) during peak growing season in April through October. These images were then atmospherically corrected and cloud-masked using ACOLITE. Afterward, they were rasterized in R and underwent the previously described pre-processing steps (Sect 2.3) to ensure compatibility with the LCM and AGBM for prediction.

Flooding dynamics can interfere with tracking land cover change by partially covering soil and vegetation. Therefore, change should be compared across growing season images with the lowest tides. To select optimal images to use in annual land cover change, we first calculated vegetation cover. The annual images with the highest total vegetation cover were assumed to have the lowest tides and were selected to represent that year's land cover. Further, we downloaded NOAA tide level data to be used as confirmatory data for flooding throughout the 8-year period (Center for Operational Oceanographic

Products and Services, n.d.). The AGBM was then also applied to the same images selected for land cover in order to generate site-wide annual biomass change. These time series were used to quantify land cover (% of RAC) and AGB (g m^{-2}) change through time. We also calculated the area in hectares covered by each land cover by multiplying the number of pixels by pixel area per class. This provided a visualization of change in vegetation, bare soil, and water coverage across an 8-year time period.

We then applied generalized additive models (GAMs) to investigate how spatial and temporal factors influenced variation in the modeled biophysical metrics, land cover, and AGB across RACs. GAMs are well-suited for ecological time series data as they offer a flexible approach to modeling complex, nonlinear relationships without imposing strict assumptions about their form. This made them ideal for visualizing how biophysical metrics responded to covariates such as year, spatial location, and restoration age using partial effect plots.

To assess temporal trends of vegetation cover across RACs, we modeled the change in proportion of vegetated area in hectares per RAC per year from 2016 to 2023 using a GAM with a gaussian error distribution and identity link function. The final model included a smooth term for year using a tensor product basis with a fixed basis dimension ($k = 8$), and parametric terms for RAC identity. This formulation allowed for flexible modeling of non-linear temporal patterns across all RACs, while also accounting for differences among RACs as fixed effects. The same GAM structure was used to assess patterns in AGB across RACs, where mean AGB per year per RAC served as the response variable, modeled using a Gaussian error distribution. Smoothing parameters in all models were estimated using restricted maximum likelihood (REML), which balances goodness-of-fit with model complexity to prevent overfitting.

We also explored alternative model structures, including one with separate smooths over time for each RAC and another using a binomial error distribution with a logit link to directly model proportional

vegetation cover. However, these alternatives either did not improve model fit or added unnecessary complexity.

3. RESULTS

3.1 Assemble the datasets needed for model building, including ground-truth and remote sensing data

Field Data

We conducted three field visits in the falls of 2022, 2023, and 2024. These visits resulted in field measures at 189 plots across all three RACs (Table 3). This project also leveraged collaborator data that included 576 plots of coastal marsh collected in Port Aransas, TX (Table 3). These collaborator data were collected similarly in all ways, except that they did not include biomass data, and the data also spanned a salinity gradient from fresh to salt marsh habitats.

In Galveston, compared to mid RACs, plot-level field data from old RACs had a 21% increase in vegetation cover and 36% increase in AGB (Table 3). However, old RACs had 29% lower RTK-measured elevation (Table 3) versus mid RACs. Comparisons between the Galveston and Port Aransas data showed 34% higher vegetation cover in Galveston and 38% higher RTK-measured elevations in Port Aransas than in Galveston due to differences in experimental design and sampling locations.

Table 3. Means (± standard error) from 1-m^2 plot-level field measurements across all restoration age groups and data collections, including data collected by this study in Galveston, TX, and leveraged collaborator data from Port Aransas, TX.

Wetland Type	Vegetation Cover (%)	Bare Ground Cover (%)	RTK Elevation (m)	Aboveground Biomass (g m^{-2})	Number of Samples (N)
Overall Site Means					
Galveston	51 ± 3.1	49 ± 3.1	0.24 ± .02	181 ± 14	189
Port Aransas	36 ± 1.3	43 ± 1.6	0.33 ± .01	N/A	576

Wetland Type	Vegetation Cover (%)	Bare Ground Cover (%)	RTK Elevation (m)	Aboveground Biomass (g m-²)	Number of Samples (N)
Galveston Restoration Age Means					
Mid	43 ± 3.6	57 ± 3.6	0.24 ± .03	127 ± 21	63
Old	52 ± 4.5	48 ± 4.5	0.17 ± .02	233 ± 29	63
Ref	54 ± 4.2	46 ± 4.2	0.24 ± .02	183 ± 19	63

Remote Sensing Data

S2 data downloaded for model building included 11 total Level 1C S2 satellite images, which provided complete coverage of both data collection sites in Port Aransas and Galveston. For our DEM data, 5 LiDAR-derived images collected in 2018 were used to build our DECM. After combining the Galveston and Port Aransas data, we had 765 plots. Through filtering to find the least flooded images, pixel averaging identical reflectance data, and only using elevations above 0 m, we had 411 plots from the 2018 images, a 46% data decrease. For the LCM, we used 5 images collected from 2021 to 2023 to match field data collection dates. After filtering and averaging these images, we were left with 572 plots, a 25% decrease.

3.2 Build remote sensing-derived models for monitoring restoration trajectory

Digital Elevation Correction Model Performance

We assessed the DECM's predictor importance from a feature importance plot (Figure 3), which ranked DEM data as the strongest predictor, followed by the S2 bands 1 and 12. Two SRs were used as predictors and included ratios of bands 8 and 12, as well as a ratio of bands 5 and 6. Before correction, digital elevation compared to RTK measured elevation had an RMSE of .29-m (Figure 3A). After applying the correction model, this error was reduced to an RMSE of 0.12-m (a 60% reduction) and a mean absolute error (MAE) of 0.09-m (Figure 3B).

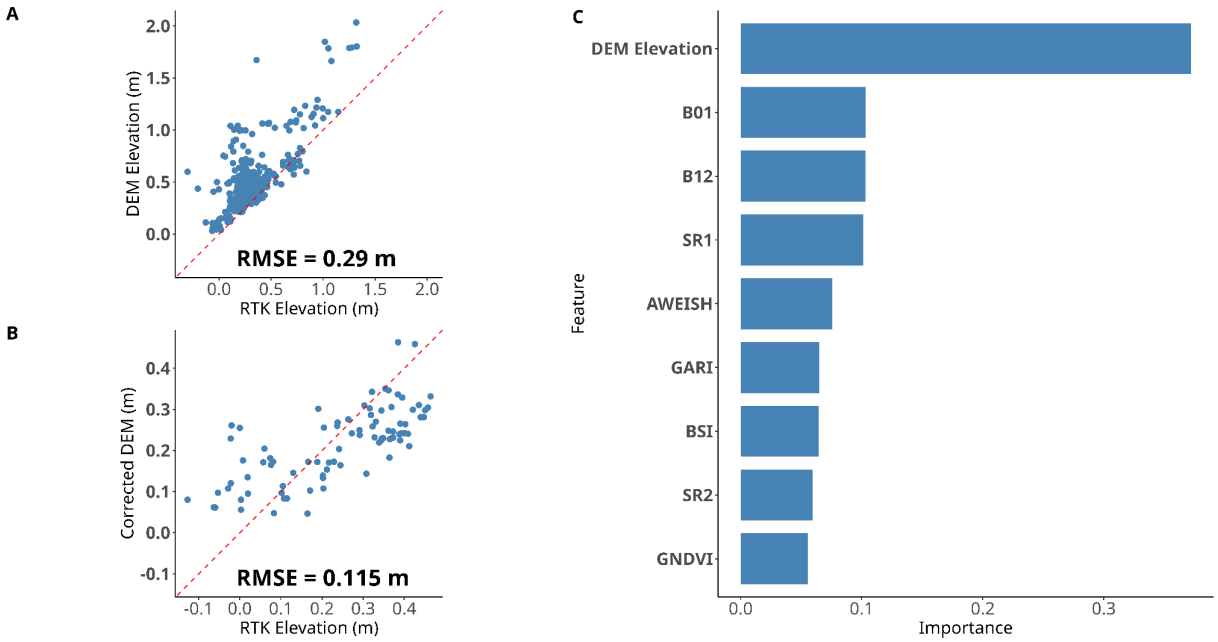

Figure 3. (A). The relationship between observed RTK elevation (m) and model-corrected elevation for the novel testing data, where S2 surface reflectance and the original DEM data served as predictors. The DECM was used to correct DEM data on a pixel basis across mounds and ref RACs. (B). Root Mean Squared Error (RMSE) is reported as 0.12-m and mean absolute error (MAE) as 0.09-m. The model is limited to elevations above 0-m NAVD88, as flooding reduces the utility of terrestrial LiDAR-derived DEMs. (C). Feature importance plot for 9 variables (features) included in the model. DEM elevation was the strongest predictor, and S2 bands, VIs, and SRs also contributed.

Land Cover Model (LCM) Performance

The LCM identified S2 pixels as water, vegetation, or bare soil. Model performance was assessed using a confusion matrix, where overall training and testing accuracy were each 90% (Table 4). In this model, sensitivity is the ability to detect true positives for land cover, and specificity is the ability to detect true negatives. Bare soil was the most accurately predicted cover, and had the highest sensitivity and specificity in the testing set at 100% and 97%, respectively. Water was the most difficult class to predict, and had 86% sensitivity and 93% specificity in testing data (Table 4). NDVI was the most important predictor for distinguishing land cover classes, followed by band 3 and GARI (Figure 4).

Table 4. Land cover classification results. The LCM was used to predict cover on a pixel basis across mounds and ref RACs. Sensitivity and specificity are the accuracy of classifying true positive and true negative pixels, respectively; accuracy is total model accuracy; N is sample

size, in terms of pixels classified. Training data were used to fit the model, while testing data were an independent subset totally withheld from training to evaluate model performance.

Data	Accuracy	Sensitivity	Specificity	N	Misclassified
Training	90			353	
Bare		92	95		21
Vegetation		85	96		29
Water		96	94		18
Testing	90			192	
Bare		100	97		4
Vegetation		88	93		18
Water		86	93		16

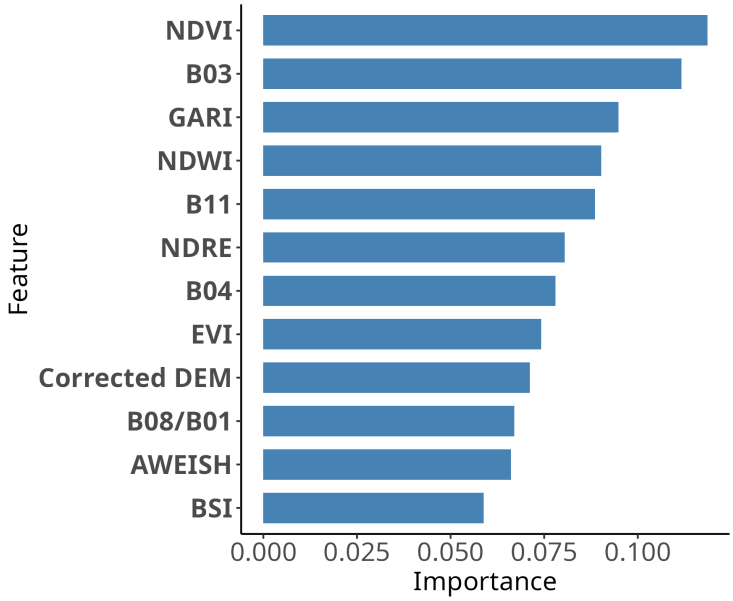

Figure 4. LCM feature importance plot. NDVI was the most important feature for predicting land cover on S2. Band 3 (green band) and GARI were the second and third most important features. SR2 includes band 8 over band 1.

Aboveground Biomass Model (AGBM) Performance

The AGBM used predictors derived from S2 satellite imagery and DEMs. The most important predictors were band 2 (blue) and band 3 (green), followed by an SR of band 12 to band 6 (Figure 5A). When evaluated on the testing dataset, the model achieved an RMSE of 82.4 g m^{-2}, a normalized RMSE (nRMSE) of 0.14, an MAE of 48.5 g m^{-2}, and an R^2 of 0.82 (Figure 5B).

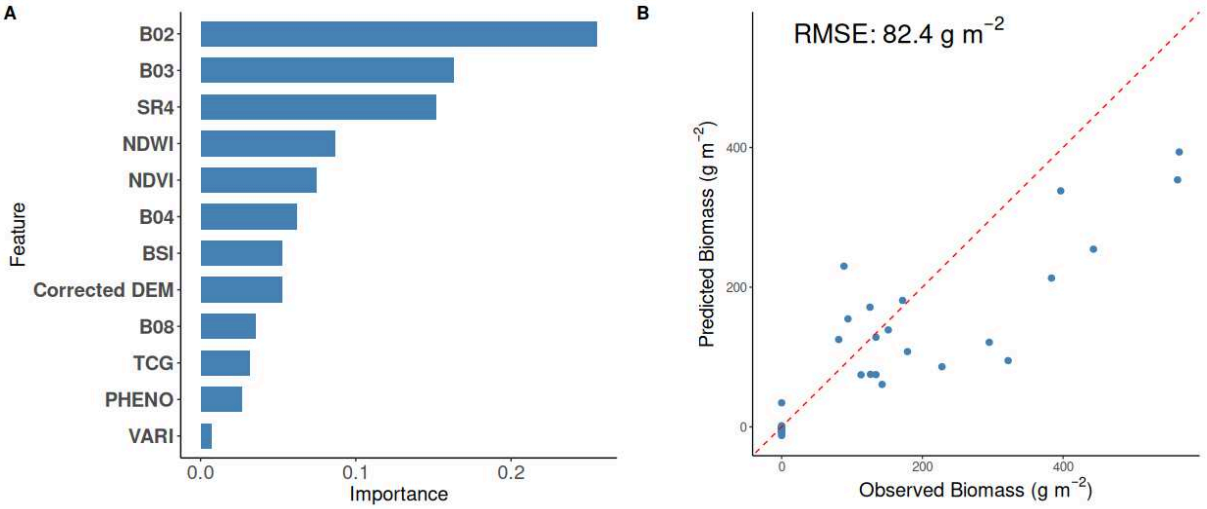

Figure 5. (A.) Feature importance and testing data performance for the AGBM. S2 bands 2 and 3 were the strongest predictors. Other notable predictors include corrected DEM data, NDVI, and VARI, which are common VIs used for vegetation detection. (B.) The AGBM was used to predict AGB on a pixel basis across mounds and ref RACs. Testing data had an RMSE of 82.4 g m^{-2} and an MAE of 48.5 g m^{-2} but had a trend of somewhat underpredicting biomass at larger masses.

3.3 Generate remote sensing-derived time series to confirm observed spatial differences between restoration age classes.

Digital Elevation Correction Model (DECM) Application

The DECM was applied to the 2018 LiDAR-derived DEM to reduce error and improve the accuracy of elevation estimates across the restoration site. Elevations above 1.1 m were removed to restrict analysis to the wetland extent (Figure 6A). Mean elevation significantly differed among RACs, as a GAM indicated that site class and spatial location significantly explained variation in elevation ($p < 0.001$, adjusted $R^2 = 0.575$). The ref RAC had the highest mean elevation (0.50 m), followed by the mid (0.28 m) and old RACs (0.26 m) (Figure 6B).

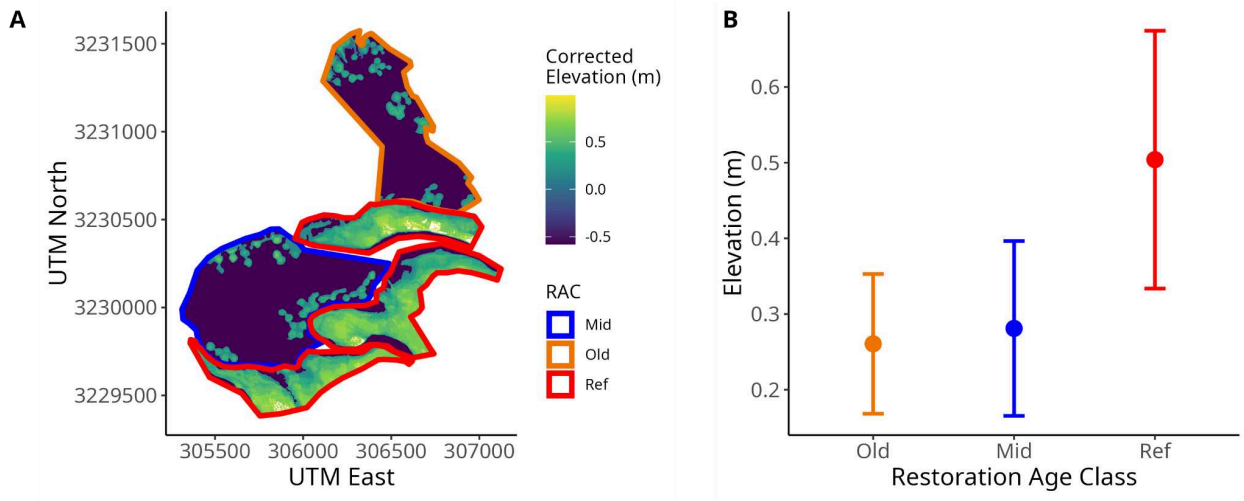

Figure 6. (A.) The final corrected DEM raster for the restoration site, with elevations above 1.1 meters removed to focus analysis on the wetland area. (B.) A point plot showing mean elevations ± standard deviations. Ref RAC had the highest mean elevation (0.50 ± 0.17 m), followed by mid (0.28 ± 0.12 m) and old RACs (0.26 ± 0.09 m).

Land Cover Model Time Series Application

On average, the old RAC had 8.1 ± 2.7 ha (mean±standard deviation) of vegetation cover, with water and bare soil averaging 32.5 ± 2.7 and 0.1 ± 0.2 ha, respectively. The ref RAC had a mean vegetation cover of 45.5 ± 2.8 ha, 16.5 ± 2.0 ha of water, and 3.2 ± 3.4 ha of bare soil. The mid RAC had an average vegetation cover of 7.4 ± 2.8 ha, water spanning 48 ± 1.4 ha, and bare soil covering 0.64 ± 0.5 ha on average.

Initial land cover areas are not directly comparable across RACs due to differences in total area covered by the RACs, differences in the steepness of the elevation gradients from marsh edge to marsh interior, and the subsequent area covered by plant communities that are arrayed along elevation zones. Therefore, baseline proportions may reflect geomorphic structural differences rather than ecological resiliency. However, temporal changes in land cover proportions are informative for assessing whether restored sites are on trajectories similar to reference conditions.

We used a GAM to explore how the change in proportion of vegetation cover varied over space and time across RACs. The model explained a low level of the variance with an adjusted R^2=-0.09 and deviance

explained=5.1%. Parametric coefficients showed that the change in vegetation proportion did not differ significantly between RACs ($p>0.5$). The temporal smooth term was also not significant ($p=0.48$), and there was no evidence of a RAC * year interaction effect. While an examination of means showed an inverse relationship between vegetation and water cover, changes across years were small and non-significant. This can be seen at mid RACs between 2019 and 2020, where vegetated pixels decreased by 2.1 ha, while water pixels increased by 2.0 ha. Similarly, at old RACs from 2018 to 2019, vegetation cover expanded by 5.4 ha, coinciding with a 5.5 ha decline in water cover. In general, vegetation cover remained relatively stable over the 8 years across the RACs.

While changes in vegetation were not statistically significant, the changes observed could still have ecological implications. We observed longer-term patterns of vegetation converting to water at old RACs (Figure 7). At the old RAC, 37% of pixels in the old RAC in 2016 had transitioned from vegetation to water by 2023 (Figure 7A). Of these, 73% remained in their transitioned state in both 2022 and 2023, indicating stability. In other words, most vegetation pixels that were converted to water remained as water. In contrast, only 14% of pixels in the mid RAC and 6% in ref RACs underwent this vegetation-to-water transition from 2016 to 2023 (Figure 7A). However, in the mid RAC, transitions from bare soil to vegetation, and water to vegetation made up 15% of vegetated pixels in 2023, making vegetation loss negligible.

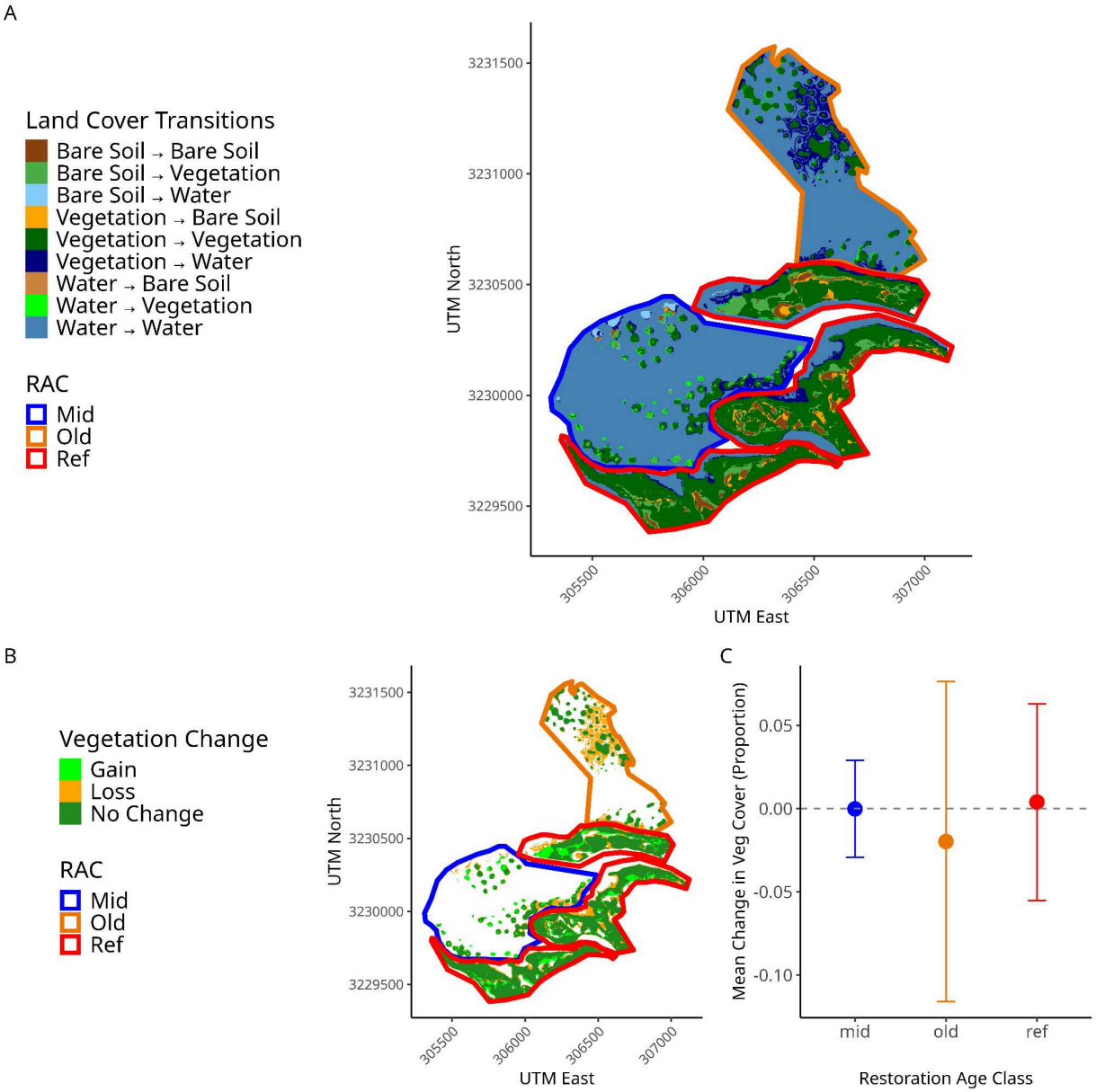

Figure 7. (A.) Land cover transitions that occurred from the 2016 land cover raster to the 2023 land cover raster. In total, across all RACs, 11.8 ha of vegetation was lost to water. The old RAC lost the most with 6.3 ha converted to water. Ref RACs converted 4.8 ha of bare soil to vegetation by 2023, compared to 0.9 ha in mid RACs. (B.) Vegetation gain and loss across RACs. Overall, 14.0 ha of vegetation were lost while 7.5 ha were gained across all RACs. Net loss was 6.5 ha of vegetation. (C.) Mean change in proportion of vegetation cover ± standard deviation across the 8-year period from 2016 to 2023 was slight and did not differ among RACs.

Aboveground Biomass Model Application

The AGBM was applied to cloud and water-masked S2 imagery from 2016 to 2023. Over this eight-year period, the old RAC had the highest overall mean AGB (221 ± 39.6 g m^{-2}) (mean ± standard deviation), with a peak of 274 g m^{-2} in 2017. The mid RAC had a mean AGB of 201 ± 47.0 g m^{-2}, reaching a maximum of 277 g m^{-2} in 2020. Reference RACs exhibited the lowest mean AGB (180 ± 41.3 g m^{-2}), with a maximum of 246 g m^{-2} in 2017. Visual inspection of these trends suggests a noisy decline in AGB at old sites and a slight increase at mid-aged sites over time (Figure 8B).

We assessed the ecological significance of these AGB trends from a GAM with mean AGB (g m^{-2}) per year per restoration age class (RAC) as the response variable. The model explained a moderate amount of variance (adjusted $R^2 = 0.50$, deviance explained = 67%). The smooth term for year was statistically significant ($p = 0.049$), indicating evidence of temporal variation in AGB over the 8-year period (Figure 8A). However, the parametric effects of RAC were not significant ($p = 0.22$ for both old and ref RACs), suggesting no consistent differences in mean AGB among the RACs.

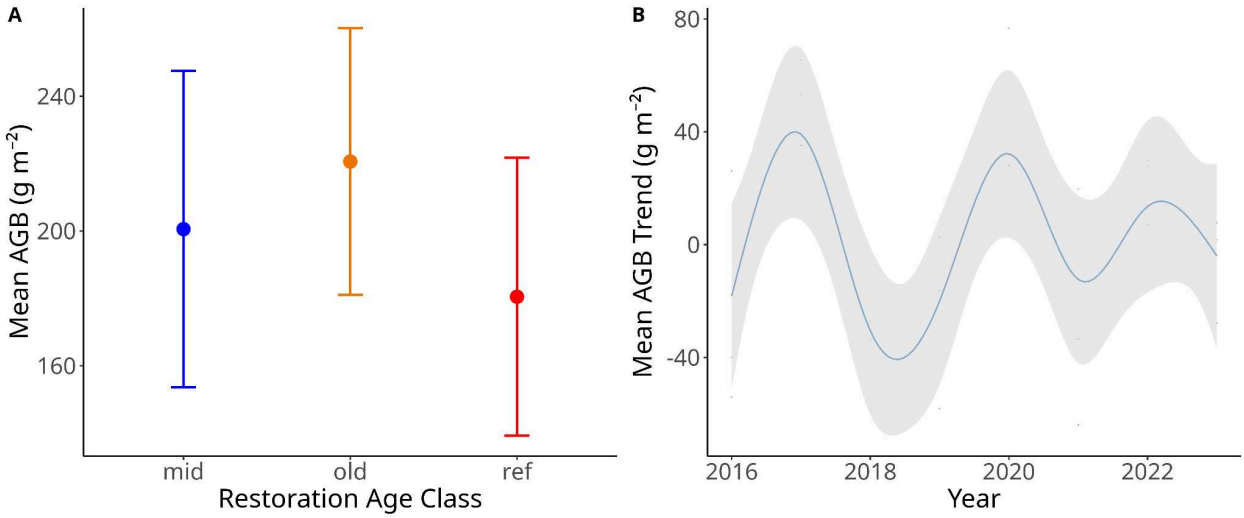

Figure 8. (A.) Mean AGB (g m^{-2}) ± standard deviation at each restoration age class (RAC). While mean AGB values were similar across sites, high variability is evident from the large standard deviations. (B.) Temporal trend of mean AGB from 2016 to 2023 predicted from a GAM, showing smoothed changes in AGB with 95% confidence intervals.

4. DISCUSSION

The performance of the models developed in this study demonstrates that remote sensing-based monitoring offers an effective and scalable approach to monitoring wetland restoration by accurately tracking wetland elevation, land cover, and productivity. Incorporating ground-truth data from comprehensive fieldwork substantially enhanced model validation and enabled robust evaluation from novel test data. Integration of field-measured RTK elevations through the DECM substantially increased DEM accuracy. The LCM, informed by field-measured vegetation cover, successfully captured land cover trends from 2016 to 2023. When paired with the AGBM, this time series can help assess the restoration's trajectory and is a commonly used method in wetland monitoring studies (Demarquet et al., 2023; Naidoo et al., 2019). These results can be applied to new time periods and coastal restorations with low cost and underscore the efficiency and practicality of using remote sensing to support long-term wetland restoration monitoring.

4.1 Model Performance Discussion

The DECM greatly improved elevation accuracy, reducing error to an RMSE of 0.115 m, which could provide insights into microtopographic controls on wetland function. Our data suggested that existing DEMs were biased high in non-flooded vegetated areas before correction. Suchrow et al. (2010) and Adams (1963) both showed that minor elevation changes affect the extent and composition of vegetated areas due to varying tolerances to inundation and salinity. These findings underscore the importance of high-resolution elevation data when assessing wetland dynamics. Hladik and Alber (2012) further reinforced this by showing that correcting DEMs is important in tidal marshes, and can improve elevation accuracy, leading to better representation of vegetation patterns and subsequently, vertical and horizontal marsh expansion or erosion. Because wetland vegetation responds so sensitively to microtopographic variation, even slight improvements in elevation data can enhance ecological interpretation and modeling (Hladik & Alber, 2012). The value of this correction step was shown in the LCM and AGBM, where corrected DEM data proved to be an important predictor.

Important indices for the DECM included uncorrected DEM data, S2 bands, and derived indices. Uncorrected DEM data predictably carried the most importance (Figure 3C), while it needed improvement for wetland systems, it still provided valuable baseline data and is commonly used in other systems (Lefsky et al., 2002). Other predictors, such as AWEISH, bands 1 and 12, and SR1 (band 8/band 2) (Figure 3C), most likely were key in highlighting differences in moisture content and vegetation structure, which can inform topography (Feyisa et al., 2014; Suchrow & Jensen, 2010). Vegetation can intercept the LiDAR signal before it reaches the ground surface (Rosso et al., 2006; Schmid et al., 2011), and denser vegetation provides greater interception. Finally, the LiDAR sensors used for this project, the Riegl R680i and the R780i, operate at NIR wavelengths, which cannot penetrate water (Fernandez-Diaz et al., 2014; Polvivaara et al., 2024), and therefore also impact DEM estimates.

The LCM had high overall test data accuracy, 90%, and performed especially well in identifying bare soil and vegetated pixels (Table 4). The success of this model was derived from the distinct spectral signatures of the land cover classes and distinct spatial locations, which aid the model in class separation (Cho et al., 2008). Bare soil was primarily found in the ref RAC, and its small spatial variability and likely low spectral diversity could have influenced its high classification accuracy (Table 4) (Campbell, 1981). Also playing a role in high overall class accuracy was NDVI, which is well documented in the literature for its ability to separate soil and vegetation classes (Montandon & Small, 2008). GARI and S2 band 3 (green) were also high-performing predictors (Figure 4) due to their sensitivity in detecting chlorophyll content and healthy vegetation (Gitelson et al., 1996). NDWI also carried high importance due to its responsiveness to water and its content changes in vegetation canopies, which most likely helped discern wet vs dry areas (Gao, 1996).

The AGBM demonstrated strong performance with an RMSE of 82.4 g m^{-2} (nRMSE 14%) when applied to novel testing data (Figure 5B). Figure 5 shows that the model performed well for lower biomass values

but had a pattern of underprediction at higher values. A common explanation for this phenomenon is the oversaturation of reflectance in dense canopies, where optical sensors have difficulty penetrating and capturing the vertical structure of the vegetation (Lu et al., 2016). This limitation is a well-documented challenge in AGB remote sensing, as emphasized by Mutanga et al. 2023. Sampling data could have also been a factor. Machine learning models often struggle with rare observations (Krawczyk, 2016), and only 11 of 91 AGB samples had >300 g m^{-2}.

AGBM feature importance (Figure 5B) showed S2's band 2 (blue) was the strongest performing feature, followed by the green band, and SR4 (band 12/band 6). A study on S2's detection of seagrass and algae by Bannari et al. 2022 emphasized the blue band's ability to be absorbed by chlorophyll and also penetrate clear water. These features allow for soil and vegetation discrimination from water, which is very useful in highlighting vegetation in water-dominant ecosystems like wetlands. Similarly, the study also highlighted that the green band (band 3) shows high contrast between clear and turbid water and is highly reflected by chlorophyll. This is especially helpful on mounded wetland restoration features where frequent inundation occurs. The spectral properties of these bands are well-suited for isolating vegetation signatures and improving the model's ability to detect biomass across the RACs.

4.2 Model Application Discussion

After applying the DECM to the Jumbile Cove restoration site, the model revealed differences in mean elevations between mound features (old and mid RACs) and the ref RAC (Figure 6B). These differences can most likely be explained by multiple vertical processes. Vertical marsh subsidence from groundwater withdrawal is what initially degraded these wetlands and could still be impacting restoration mounds (White & Tremblay, 1995). Additionally, natural settling of the dredged material used to construct the mounds could result in additional elevation loss due to soil compaction (Cahoon, 2024; Kaye & Barghoorn, 1964). Healthy coastal wetlands can resist this elevation loss through a positive feedback loop driven by tidal sedimentation and organic matter accumulation to vertically accrete soil and maintain elevation relative to sea level rise (Callaway et al., 1996; Stevenson et al., 1986). However, when sea

level rise exceeds the pace of accretion, this can cause vertical marsh subsidence, increased inundation frequency, and salinity stress, which can alter vegetation distribution (Morris et al., 2002). The RAC elevation differences could be a result of one or all of these factors.

Due to limited DEM availability, elevation could not be tracked over time. However, using a space-for-time substitution, the old RAC retained a similar elevation to the mid RAC (Figure 6B) despite being constructed 11 years earlier, suggesting that time is not an important component of elevation change, and dredge material settling or some other initial condition may therefore be a more likely explanation. The availability of NAVD88 benchmarked bathymetric LIDAR and more frequent LiDAR missions could greatly improve the DECM and allow for more monitoring of more frequent changes.

While we were able to significantly reduce DEM error, the DECM has limitations. Due to the use of terrestrial LIDAR and the lack of an available bathymetric LIDAR that can be seamlessly integrated into the NAVD88 vertical datum, we limited the DECM to only correct DEM data >0 m NAVD88 (excluding upland areas and areas covered by water). As a result, low elevation mounds that are permanently inundated remained uncorrected, which could exclude key areas of the restoration from analysis. This may limit the use of the DECM approach in low elevation areas where vegetation types are naturally permanently flooded, such as seagrass beds or freshwater ponds (Fernandez-Diaz et al., 2014).

After applying both the LCM and AGBM to selected images across the 8-year period, we were able to highlight spatial and temporal differences between RACs. Ecological responses to changes in drivers such as elevation and hydrology (Kirwan et al., 2010; Kirwan & Guntenspergen, 2010; Morris et al., 2002), and restoration design could be responsible for these observed differences. While AGB change was observed over time, it was not significantly different among RACs. The temporal trajectory of AGB (Figure 8A) was complex, suggesting that AGB fluctuates in response to long-term shifts in hydrodynamics, as others have observed (Zweig & Kitchens, 2008). A forthcoming study by Runion et al.

(2025, in press) demonstrates the complexity of AGB for monitoring purposes, as AGB increases can be caused by increased flooding (Kirwan & Megonigal, 2013; Runion et al., 2025). Increasing AGB often accompanies belowground biomass declines, and is sometimes a forewarning of incipient marsh subsidence and drowning (Runion et al., 2025). Thus, interpreting these responses requires consideration of a suite of biophysical responses, rather than any single variable.

The LCM helped reveal restoration trajectories by quantifying how bare soil, water, and vegetation cover fluctuate over time (Figure 7). Reference RACs encompassed substantially more area, and thus had greater cover of vegetation and soil than the other RACs. In general, across all RACs, land cover changes were minor, and cover was relatively stable through time. One exception was bare soil, which exhibited greater spatial and temporal heterogeneity in the ref RAC than in other RACs, where it remained static (Figure 7A). This structural variability may facilitate vegetation dispersal and offer potential refuge zones for upland marsh migration in response to sea level rise (Raabe & Stumpf, 2016; Schieder et al., 2018). Vegetation transitions to water were minimal in the reference RAC (6%) compared to the old RAC, where 37% of pixels had converted to water by 2023. Notably, many of these transitions in the old RAC occurred in areas between mounds, potentially indicating the detection of seagrass in shallow water in the early images. Their disappearance by 2023 suggests that rising sea levels may have increased water depth to the point where spectral signatures of submerged vegetation became undetectable (Bannari et al., 2022; Pinnel et al., 2005) or that seagrass declined due to deteriorating conditions in light availability and water depth. Additionally, moderate losses in mound area in the old RAC (Figure 7A) point to erosion or submergence processes degrading restoration mounds, but evidence for statistically significant losses in mound area was not detected. The slight increase in vegetation cover in the mid RAC over time (Figure 7A) may be attributed to its more recent construction and slightly higher elevation, as well as the restoration design in which vegetation was initially planted along the mound perimeters and subsequently expanded inward. Finally, the moderate area losses in some mounds may have been deposited in more interior wetland areas by wave action and contributed to the increases in bare soil sometimes observed in

the ref RAC. This supports that ref RACs are aligning with the intended restoration design (Davis et al. 2024), where mounded features provide a buffer to wind and waves, slowing lateral erosion and allowing ref RACs to maintain vegetated marsh areas.

While the LCM and AGB produced promising results, several limitations remain. One of the primary challenges for the model was mound flooding. Water significantly dampens spectral reflectance due to its high absorption of light (Dekker et al., 2001; Gould et al., 2001), which, along with frequent cloud cover, restricts the availability of suitable S2 imagery for model prediction. By comparing surface reflectance with on-site water depth measurements, we found that light attenuation begins at approximately 20–25 cm of water depth. As a result, lower elevation mounds often become undetectable to the S2 sensor during high tide events when water levels exceed this threshold. Incorporating synthetic aperture radar data (SAR), which can better penetrate clouds and shallow water, could improve the model's ability to detect inundated mounds (Sahour et al., 2022). Future studies should consider incorporating SAR of various wavelengths, such as Sentinel-1 C-band SAR or L-band SAR from the forthcoming NISAR data (Jet Propulsion Laboratory, n.d.). However, including multiple data products can increase model complexity and computation time, and can reduce prediction frequency if all products are needed for prediction.

The AGBM faced similar limitations as the LCM, with flooding posing a major challenge to accurate biomass estimation. To mitigate these effects, it was necessary to mask water pixels prior to model prediction. We also used images with the highest growing season vegetated area for annual biomass predictions, as an effort to minimize the spectral dampening and biomass underestimation caused by minor tidal flooding. However, since AGB also varies seasonally, our yearly image selection window (April-October) could allow for seasonal differences in canopy development that could impact results. While these limitations needed to be addressed, the AGB model can still provide useful information for management despite these restrictions.

Overall, our results emphasize the importance of considering both restoration design and ecological context when evaluating project success. At Jumibile Cove, reference sites exhibited relatively stable vegetation cover and increasing biomass levels, while restored sites, particularly mid-aged ones, demonstrated encouraging signs of vegetation expansion and biomass accumulation. These patterns suggest that restoration mounds, to date, are supporting resilient vegetated communities. Based on our RAC-wide assessments, changes in vegetation proportions and similarly increasing mean AGB across years suggest that vegetation provisioning services are broadly comparable among RACs and are progressing along similar ecological trajectories. Continued tracking of elevation and inundation frequency will be critical for sustaining these gains and guiding adaptive management under changing environmental conditions. This is especially important in the old RAC, where the elevated rate of vegetation-to-water transitions observed highlights a potential vulnerability to long-term hydrologic pressures such as sea level rise or land subsidence. These mounds also had much lower mean elevation than reference RACs. This indicates that while the mounds remain ecologically functional, their long-term physical stability may be at risk. Continued monitoring is particularly important in these older restoration mounds, where elevation loss or erosion may threaten the persistence of restored features. To combat this potential degradation, we recommend management actions such as additional vegetation planting, installation of erosion control structures, or increasing mound elevation through thin-layer soil placement.

The remote sensing monitoring framework developed in this study demonstrates strong potential for supporting wetland restoration management across diverse systems. By leveraging high-resolution and freely available Sentinel-2 imagery and elevation data, the models achieved high classification accuracy and effectively captured key trends in biophysical parameters such as elevation, land cover, and AGB, offering insight into restoration trajectories over time. The final results also suggested the potential for spatial interactions among adjacent areas, with more exposed marshes potentially buffering interior marshes. Remote sensing enables the detection of spatial and temporal patterns at scales far beyond traditional 1 m^2 field plots, allowing for a more comprehensive understanding of landscape-level

restoration dynamics. While field validation and expert interpretation remain essential, this approach significantly reduces the labor and cost typically associated with long-term monitoring. By applying this scalable and cost-effective framework, managers can more readily detect emerging restoration challenges and make timely, data-driven decisions that enhance the likelihood of restoration success.

REFERENCES

Adam, P. (1993). *Saltmarsh Ecology*. Cambridge University Press.

Bannari, A., Ali, T. S., & Abahussain, A. (2022). The capabilities of Sentinel-MSI (2A/2B) and Landsat-OLI (8/9) in seagrass and algae species differentiation using spectral reflectance. *Ocean Science*, *18*(2), 361–388. https://doi.org/10.5194/os-18-361-2022

Bockelmann, A.-C., Bakker, J. P., Neuhaus, R., & Lage, J. (2002). The relation between vegetation zonation, elevation and inundation frequency in a Wadden Sea salt marsh. *Aquatic Botany*, *73*(3), 211–221. https://doi.org/10.1016/S0304-3770(02)00022-0

Brasher, M. G., & Blvd, C. (2015). *Review of the Benefits of Marsh Terraces in the Northern Gulf of Mexico*.

Burger, J., Niles, L., & Clark, K. E. (1997). Importance of beach, mudflat and marsh habitats to migrant shorebirds on Delaware Bay. *Biological Conservation*, *79*(2), 283–292. https://doi.org/10.1016/S0006-3207(96)00077-8

Cahoon, D. R. (2024). Measuring and Interpreting the Surface and Shallow Subsurface Process Influences on Coastal Wetland Elevation: A Review. *Estuaries and Coasts*, *47*(7), 1708–1734. https://doi.org/10.1007/s12237-024-01332-z

Callaway, J. C., Nyman, J. A., & DeLaune, R. D. (1996). *Sediment Accretion In Coastal Wetlands: A Review And A Simulation Model Of Processes*.

Campbell, J. B. (1981). Spatial Correlation Effects upon Accuracy of Supervised Classification of Land Cover. *Photogrammetric Engineering*.

Center for Operational Oceanographic Products and Services. (n.d.). *Water Levels—NOAA Tides & Currents* [Dataset]. Retrieved June 5, 2025, from https://tidesandcurrents.noaa.gov/waterlevels.html?id=8771486

Cho, H. J., Kirui, P., & Natarajan, H. (2008). Test of Multi-spectral Vegetation Index for Floating and Canopy-forming Submerged Vegetation. *International Journal of Environmental Research and Public Health*, *5*(5), Article 5. https://doi.org/10.3390/ijerph5050477

Davis, J., LeClaire, A., Bost, M., Walker, Q., & Giannelli, R. (2024). Site Report: Jumbile Phase II. *US DOC NOAA NOS National Centers for Coastal Ocean Science (NCCOS)*.

De Groot, D., Brander, L., & Finlayson, C. M. (2018). Wetland Ecosystem Services. In C. M. Finlayson, M. Everard, K. Irvine, R. J. McInnes, B. A. Middleton, A. A. Van Dam, & N. C. Davidson (Eds.), *The Wetland Book* (pp. 323–333). Springer Netherlands. https://doi.org/10.1007/978-90-481-9659-3_66

Dekker, A., Brando, V., Anstee, J., Pinnel, N., Kutser, T., Hoogenboom, E., Peters, S., Pasterkamp, R., Vos, R., Olbert, C., Malthus, T., VanDerMeer, F., & DeJong, S. (2001). Imaging Spectrometry of Water. *Imaging Spectrometry: Basic Principles and Prospective Applications*, *4*, 307–359. https://doi.org/10.1007/978-0-306-47578-8_11

DeLaune, R. D., & Pezeshki, S. R. (1994). The Influence of Subsidence and Saltwater Intrusion on Coastal Marsh Stability: Louisiana Gulf Coast, U.S.A. *Journal of Coastal Research*, 77–89.

Demarquet, Q., Rapinel, S., Dufour, S., & Hubert-Moy, L. (2023). Long-Term Wetland Monitoring Using the Landsat Archive: A Review. *Remote Sensing*, *15*(3), Article 3. https://doi.org/10.3390/rs15030820

Fernandez-Diaz, J. C., Glennie, C. L., Carter, W. E., Shrestha, R. L., Sartori, M. P., Singhania, A., Legleiter, C. J., & Overstreet, B. T. (2014). Early Results of Simultaneous Terrain and Shallow Water Bathymetry Mapping Using a Single-Wavelength Airborne LiDAR Sensor. *IEEE Journal of Selected Topics in Applied Earth Observations and Remote Sensing*, *7*(2), 623–635. https://doi.org/10.1109/JSTARS.2013.2265255

Feyisa, G. L., Meilby, H., Fensholt, R., & Proud, S. R. (2014). Automated Water Extraction Index: A new technique for surface water mapping using Landsat imagery. *Remote Sensing of Environment*, *140*, 23–35. https://doi.org/10.1016/j.rse.2013.08.029

Gao, B. (1996). NDWI—A normalized difference water index for remote sensing of vegetation liquid water from space. *Remote Sensing of Environment*, *58*(3), 257–266. https://doi.org/10.1016/S0034-4257(96)00067-3

Giri, C., Ochieng, E., Tieszen, L. L., Zhu, Z., Singh, A., Loveland, T., Masek, J., & Duke, N. (2011). Status and distribution of mangrove forests of the world using earth observation satellite data. *Global Ecology and Biogeography*, *20*(1), 154–159. https://doi.org/10.1111/j.1466-8238.2010.00584.x

Gitelson, A. A., Kaufman, Y. J., & Merzlyak, M. N. (1996). Use of a green channel in remote sensing of global vegetation from EOS-MODIS. *Remote Sensing of Environment*, *58*(3), 289–298. https://doi.org/10.1016/S0034-4257(96)00072-7

Gould, R. W., Arnone, R. A., & Sydor, M. (2001). Absorption, Scattering, and Remote-Sensing Reflectance Relationships in Coastal Waters: Testing a New Inversion Algorith. *Journal of Coastal Research*, *17*(2), 328–341.

Guo, M., Li, J., Sheng, C., Xu, J., & Wu, L. (2017). A Review of Wetland Remote Sensing. *Sensors*, *17*(4), Article 4. https://doi.org/10.3390/s17040777

Hladik, C., & Alber, M. (2012). Accuracy assessment and correction of a LIDAR-derived salt marsh digital elevation model. *Remote Sensing of Environment*, *121*, 224–235. https://doi.org/10.1016/j.rse.2012.01.018

Hladik, C., Schalles, J., & Alber, M. (2013). Salt marsh elevation and habitat mapping using hyperspectral and LIDAR data. *Remote Sensing of Environment*, *139*, 318–330. https://doi.org/10.1016/j.rse.2013.08.003

Jet Propulsion Laboratory. (n.d.). *NISAR Quick Facts*. NASA-ISRO SAR Mission (NISAR). Retrieved June 5, 2025, from https://nisar.jpl.nasa.gov/mission/quick-facts

Kaye, C. A., & Barghoorn, E. S. (1964). Late quaternary sea-level change and crustal rise at Boston, Massachusetts, with notes on the autocompaction of peat. *Geological Society of America Bulletin*, *75*(2), 63–80. https://doi.org/10.1130/0016-7606(1964)75[63:LQSCAC]2.0.CO;2

Kirwan, M. L., & Guntenspergen, G. R. (2010). Influence of tidal range on the stability of coastal marshland. *Journal of Geophysical Research: Earth Surface*, *115*(F2). https://doi.org/10.1029/2009JF001400

Kirwan, M. L., Guntenspergen, G. R., D'Alpaos, A., Morris, J. T., Mudd, S. M., & Temmerman, S. (2010). Limits on the adaptability of coastal marshes to rising sea level. *Geophysical Research Letters*, *37*(23). https://doi.org/10.1029/2010GL045489

Kirwan, M. L., & Megonigal, J. P. (2013). Tidal wetland stability in the face of human impacts and sea-level rise. *Nature*, *504*(7478), 53–60. https://doi.org/10.1038/nature12856

Krauss, K. W., McKee, K. L., Lovelock, C. E., Cahoon, D. R., Saintilan, N., Reef, R., & Chen, L. (2014). How mangrove forests adjust to rising sea level. *New Phytologist*, *202*(1), 19–34. https://doi.org/10.1111/nph.12605

Krawczyk, B. (2016). Learning from imbalanced data: Open challenges and future directions. *Progress in Artificial Intelligence*, *5*(4), 221–232. https://doi.org/10.1007/s13748-016-0094-0

Lefsky, M. A., Cohen, W. B., Parker, G. G., & Harding, D. J. (2002). Lidar Remote Sensing for Ecosystem Studies: Lidar, an emerging remote sensing technology that directly measures the three-dimensional distribution of plant canopies, can accurately estimate vegetation structural attributes and should be of particular interest to forest, landscape, and global ecologists. *BioScience*, *52*(1), 19–30. https://doi.org/10.1641/0006-3568(2002)052[0019:LRSFES]2.0.CO;2

Lu, D., Chen ,Qi, Wang ,Guangxing, Liu ,Lijuan, Li ,Guiying, & and Moran, E. (2016). A survey of remote sensing-based aboveground biomass estimation methods in forest ecosystems. *International Journal of Digital Earth*, *9*(1), 63–105. https://doi.org/10.1080/17538947.2014.990526

McCauley, D. J., Arnold, W. J., Saxton, J. B., & Turner, C. J. (2019). Applying adaptive management and lessons learned from national assessments to address logistical challenges in the National Wetland Condition Assessment. *Environmental Monitoring and Assessment*, *191*(1), 329. https://doi.org/10.1007/s10661-019-7320-8

Meli, P., Benayas, J. M. R., Balvanera, P., & Ramos, M. M. (2014). Restoration Enhances Wetland Biodiversity and Ecosystem Service Supply, but Results Are Context-Dependent: A Meta-Analysis. *PLOS ONE*, *9*(4), e93507. https://doi.org/10.1371/journal.pone.0093507

Mendelssohn, I. A., & Morris, J. T. (2000). *Eco-Physiological Controls on the Productivity of Spartina Alterniflora Loisel | SpringerLink*. https://link.springer.com/chapter/10.1007/0-306-47534-0_5

Montandon, L. M., & Small, E. E. (2008). The impact of soil reflectance on the quantification of the green vegetation fraction from NDVI. *Remote Sensing of Environment*, *112*(4), 1835–1845. https://doi.org/10.1016/j.rse.2007.09.007

Morris, J. T., Sundareshwar, P. V., Nietch, C. T., Kjerfve, B., & Cahoon, D. R. (2002). Responses of Coastal Wetlands to Rising Sea Level. *Ecology*, *83*(10), 2869–2877. https://doi.org/10.1890/0012-9658(2002)083[2869:ROCWTR]2.0.CO;2

Mutanga, O., Masenyama, A., & Sibanda, M. (2023). Spectral saturation in the remote sensing of high-density vegetation traits: A systematic review of progress, challenges, and prospects. *ISPRS Journal of Photogrammetry and Remote Sensing*, *198*, 297–309. https://doi.org/10.1016/j.isprsjprs.2023.03.010

Naidoo, L., van Deventer, H., Ramoelo, A., Mathieu, R., Nondlazi, B., & Gangat, R. (2019). Estimating above ground biomass as an indicator of carbon storage in vegetated wetlands of the grassland biome of South Africa. *International Journal of Applied Earth Observation and Geoinformation*, *78*, 118–129. https://doi.org/10.1016/j.jag.2019.01.021

O'Connell, J. L., Mishra, D. R., Cotten, D. L., Wang, L., & Alber, M. (2017). The Tidal Marsh Inundation Index (TMII): An inundation filter to flag flooded pixels and improve MODIS tidal marsh vegetation time-series analysis. *Remote Sensing of Environment*, *201*, 34–46. https://doi.org/10.1016/j.rse.2017.08.008

Piñeiro, G., Perelman, S., Guerschman, J. P., & Paruelo, J. M. (2008). How to evaluate models: Observed vs. predicted or predicted vs. observed? *Ecological Modelling*, *216*(3), 316–322. https://doi.org/10.1016/j.ecolmodel.2008.05.006

Pinnel, N., Heege, T., & Zimmermann, S. (n.d.). *Spectral Discrimination of Submerged Macrophytes in Lakes Using Hyperspectral Remote Sensing Data*.

Polvivaara, A., Korpela, I., Vastaranta, M., & Junttila, S. (2024). Detecting tree mortality using waveform features of airborne LiDAR. *Remote Sensing of Environment*, *303*, 114019. https://doi.org/10.1016/j.rse.2024.114019

Raabe, E. A., & Stumpf, R. P. (2016). Expansion of Tidal Marsh in Response to Sea-Level Rise: Gulf Coast of Florida, USA. *Estuaries and Coasts*, *39*(1), 145–157. https://doi.org/10.1007/s12237-015-9974-y

Rasser, M. K., Fowler, N. L., & Dunton, K. H. (2013). Elevation and Plant Community Distribution in a Microtidal Salt Marsh of the Western Gulf of Mexico. *Wetlands*, *33*(4), 575–583. https://doi.org/10.1007/s13157-013-0398-9

Rosso, P. H., Ustin, S. L., & Hastings, A. (2006). Use of lidar to study changes associated with *Spartina* invasion in San Francisco Bay marshes. *Remote Sensing of Environment*, *100*(3), 295–306. https://doi.org/10.1016/j.rse.2005.10.012

Rozas, L. P., & Minello, T. J. (2001). Marsh terracing as a wetland restoration tool for creating fishery habitat. *Wetlands*, *21*(3), 327–341. https://doi.org/10.1672/0277-5212(2001)021[0327:MTAAWR]2.0.CO;2

Runion, K. D., Alber, M., Mishra, D. R., Lever, M. A., Hladik, C., & O'Connell, J. L. (2025). Early warning signs of salt marsh drowning indicated by widespread vulnerability from declining belowground plant biomass. *Proceedings of the National Academy of Sciences of the United States of America*, *122*.

Sahour, H., Kemink, K. M., & O'Connell, J. (2022). Integrating SAR and Optical Remote Sensing for Conservation-Targeted Wetlands Mapping. *Remote Sensing*, *14*(1), Article 1. https://doi.org/10.3390/rs14010159

Schieder, N. W., Walters, D. C., & Kirwan, M. L. (2018). Massive Upland to Wetland Conversion Compensated for Historical Marsh Loss in Chesapeake Bay, USA. *Estuaries and Coasts*, *41*(4), 940–951. https://doi.org/10.1007/s12237-017-0336-9

Schmid, K., Hadley, B., & Wijekoon, N. (2011). Vertical Accuracy and Use of Topographic LIDAR Data in Coastal Marshes. *Journal of Coastal Research*, *27*, 116–132. https://doi.org/10.2307/41315921

Schmidt, K. S., & Skidmore, A. K. (2003). Spectral discrimination of vegetation types in a coastal wetland. *Remote Sensing of Environment*, *85*(1), 92–108. https://doi.org/10.1016/S0034-4257(02)00196-7

Schratz, P., Muenchow, J., Iturritxa, E., Richter, J., & Brenning, A. (2019). Hyperparameter tuning and performance assessment of statistical and machine-learning algorithms using spatial data. *Ecological Modelling*, *406*, 109–120. https://doi.org/10.1016/j.ecolmodel.2019.06.002

Shi, T., & Xu, H. (2019). Derivation of Tasseled Cap Transformation Coefficients for Sentinel-2 MSI At-Sensor Reflectance Data. *IEEE Journal of Selected Topics in Applied Earth Observations and Remote Sensing*, *12*(10), 4038–4048. https://doi.org/10.1109/JSTARS.2019.2938388

Shuman, C. S., & Ambrose, R. F. (2003). A Comparison of Remote Sensing and Ground-Based Methods for Monitoring Wetland Restoration Success. *Restoration Ecology*, *11*(3), 325–333. https://doi.org/10.1046/j.1526-100X.2003.00182.x

Stevenson, J. C., Ward, L. G., & Kearney, M. S. (1986). Vertical Accretion In Marshes With Varying Rates Of Sea Level Rise. In D. A. Wolfe (Ed.), *Estuarine Variability* (pp. 241–259). Academic Press. https://doi.org/10.1016/B978-0-12-761890-6.50020-4

Suchrow, S., & Jensen, K. (2010). Plant Species Responses to an Elevational Gradient in German North Sea Salt Marshes. *Wetlands*, *30*(4), 735–746. https://doi.org/10.1007/s13157-010-0073-3

Texas Geographic Information Office. (n.d.). *Upper Coast LiDAR*. TxGIO Datahub. Retrieved June 5, 2025, from https://data.geographic.texas.gov/collection/?c=b5bd2b96-8ba5-4dc6-ba88-d88133eb6643

Tomscha, S. A., Bentley ,Shannon, Platzer ,Elsie, Jackson ,Bethanna, de Roiste ,Mairead, Hartley ,Stephen, Norton ,Kevin, & and Deslippe, J. R. (2021). Multiple methods confirm wetland restoration improves ecosystem services. *Ecosystems and People*, *17*(1), 25–40. https://doi.org/10.1080/26395916.2020.1863266

Vanhellemont, Q., & Ruddick, K. (2016). *Acolite For Sentinel-2: Aquatic Applications Of Msi Imagery*.

White, W. A., & Tremblay, T. A. (1995). Submergence of Wetlands as a Result of Human-Induced Subsidence and Faulting along the upper Texas Gulf Coast. *Journal of Coastal Research*, *11*(3), 788–807.

Wood, S. N. (2003). Thin-plate regression splines. *Journal of the Royal Statistical Society: Series B (Statistical Methodology)*, *65*(1), 95–114. https://doi.org/10.1111/1467-9868.00374

Wood, S. N. (2004a). Stable and efficient multiple smoothing parameter estimation for generalized additive models. *Journal of the American Statistical Association*, *99*(467), 673–686. https://doi.org/10.1198/016214504000000980

Wood, S. N. (2004b). Stable and efficient multiple smoothing parameter estimation for generalized additive models. *Journal of the American Statistical Association*, *99*(467), 673–686. https://doi.org/10.1198/016214504000000980

Wood, S. N. (2017). *Generalized additive models: An introduction with R* (2nd ed.). Chapman and Hall/CRC.

Zhao, Q., Bai, J., Huang, L., Gu, B., Lu, Q., & Gao, Z. (2016). A review of methodologies and success indicators for coastal wetland restoration. *Ecological Indicators*, *60*, 442–452. https://doi.org/10.1016/j.ecolind.2015.07.003

Zweig, C. L., & Kitchens, W. M. (2008). Effects of landscape gradients on wetland vegetation communities: Information for large-scale restoration. *Wetlands*, *28*(4), 1086–1096. https://doi.org/10.1672/08-96.1